Mediterranean Journal of Nutrition and Metabolism 12 (2019) 411–422
DOI:10.3233/MNM-190333
IOS Press

Synthesis and characterisation of steroidal inhibitors of α-amylase, α-glucosidase and oxidative species

Bamidele J. Okoli[a,b,*], Mthunzi Fanyana[c], James D. Habila[d], Ayo G. Rachael[d], Iloegbulam G. Ndukwe[d], Olugbemi T. Olaniyan[e] and Johannes S. Modise[c]

[a]*Department of Chemical Sciences, Faculty of Science and Technology, Bingham University, Nasarawa State, Nigeria*
[b]*Department of Chemistry, Vaal University of Technology, Southern Gauteng Science and Technology Park, Sebokeng, South Africa*
[c]*Institute of Traditional Knowledge and Traditional Medicine, Dihlare Remedy, Vaal University of Technology, Southern Gauteng Science and Technology Park, Sebokeng, South Africa*
[d]*Department of Chemistry, Ahmadu Bello University, Zaria, Nigeria*
[e]*Department of Physiology, Laboratory for Reproductive Biology and Developmental Programming, Edo University Iyamho, Edo State, Nigeria*

Received 28 May 2019
Accepted 9 September 2019

Abstract.
BACKGROUND: Management of cellular metabolism and blood glucose levels are significant in the treatment of diabetes mellitus and oxidative diseases. Consequently, steroid and peptide hormone-based drugs such as methylprednisolone and insulin have been the most effective and safe methods of treatment.
OBJECTIVE: Our study investigated the digestive enzymes and oxidative species inhibitory potentials of seven derived biologically important steroids.
METHODS: Syntheses of the steroidal inhibitors (SIs) were accomplished by functional group transformations. Characterisation of SIs was achieved by spectroscopic techniques; followed by *in-vitro* enzyme and oxidative suppression studies.
RESULTS: NMR data revealed the presence of a steroid backbone, azomethine, carbonyl, and oxymethine peaks while the vibrational bands were further confirmed by the FTIR. The enzyme suppression activities of the SIs were influenced by the presence of histidine residue and free proton groups. However, the antioxidant activities were solely dependent on the free proton groups on the steroid backbone or the number of the histidine side chain. SIs [**3**, **4**, and **6**] exhibited a potent inhibitory effect on the enzyme activities compared to SIs [**1**, **2**, **5**, and **7**], while a potent antioxidant activity was reported by SI [**5**].
CONCLUSIONS: Generally, SIs with hydroxyl and α-amino acid functionalities have a strong affinity for the enzyme active site than the substrate; hence, the hydrolysis of the α-1,4-glycosidic bonds of saccharide was hindered. *In vivo* administration of SIs [**3**, **4**, and **6**] should take into cognizance the suppression effect at doses ≤939.49 μg/mL as well as the potential to induce abnormal bacterial fermentation of undigested carbohydrates in the colon at high concentration.

Keywords: α-Amylase, α-glucosidase, antioxidant activity, enzyme suppression, histidine, steroids, diabetes mellitus

ORCID: 0000-0001-7841-683X.

*Corresponding author: Bamidele J. Okoli. Tel.: +27767619418; E-mail: okolibj@binghamuni.edu.ng.

ISSN 1973-798X/19/$35.00 © 2019 – IOS Press and the authors. All rights reserved

AUTHOR COPY

1. Introduction

Many biochemical processes are dependent on free radicals and represent an essential part of aerobic life and metabolism [1]. During cellular metabolism, reactive oxygen species (ROS) are produced in a moderate amount and some situations excessively [2]; causing oxidative stress, leading to an imbalance between pro-oxidant and antioxidant concentrations. ROS deactivates metabolic enzymes and damages essential cellular components causing tissue injury through lipid peroxidation [3], which are primary triggers of cancer, inflammation, diabetes, liver cirrhosis, cardiovascular disease, Alzheimer's, and aging [4–7]. In a study by Papas [8], shreds of evidence suggesting the involvement of ROS in the pathogenesis of various diseases were reported. The detrimental impact of the oxidative species on the biochemical system has led to the development of various antioxidants to augment the body's natural defence [9–11]. However, these supplements have been limited by their insolubility and failure to reach the target site [12–14]. This has led to the search for an efficient alternative. Recently, proteins have been investigated as natural antioxidant supplements due to the ability of constituent amino acids to donate protons. According to Arcan & Yemenicioğlu [15], amino acids such as histidine exhibit metal-chelating potentials due to the presence of the heterocyclic ring. Most of the metal-chelating amino acids are essential for the normal functioning of the digestive process, regulates gastrointestinal activity, act as a neurotransmitter and regulates the discharge of gastrin [16]. In this study, we attempted to couple histidine to the C-**3** and/or C-**17** of the steroid backbone; to enhance bio-functionality and lipid-solubility as well as to explore the capacities to suppress oxidative species and modulate the activity of α-amylase and α-glucosidase.

2. Experimental

2.1. Physical and spectral analysis of steroidal inhibitors (SIs)

The melting points of the steroid derivatives were determined on a Stuart digital apparatus (model SM30, Staffordshire, UK), while percentage composition of the carbon, hydrogen, and nitrogen were estimated using an elemental analyser (LECO, Lakeview, MI). The FT-IR spectra were scanned in the range of 400–4000 cm^{-1} (PerkinElmer Spectrum 400, Waltham, MA), and the ^{1}H (400 MHz) and ^{13}C (100 MHz) spectra were traced on an NMR spectrometer (Agilent Technologies VnmrJ3, Woodland, CA). The electronic absorption spectra were obtained using a UV-VIS spectrophotometer scanning between 200–800 nm in a 1 cm quartz cell (Agilent Technologies Cary 60, Santa Clara, CA).

2.2. Synthesis of the SIs (1–7)

SI [1]: Approximately 0.5 mL of chromic acid solution was introduced into a 100 mL flask containing 5.17 mmoles methanolic cholesterol solution fitted with a condenser. The mixture was stirred and refluxed for 5 h at 65°C; afterward, the aqueous phase was extracted with dimethylformamide (2 × 10 mL) and allowed to dry over anhydrous Na_2SO_4 to give a green crystalline solid.

SI [2]: Chloroform-ethyl ether solution of trans-androsterone (6.9 mmoles) was introduced into an oven-dried 100 mL three-necked flask containing $LiAlH_4$, (0.72 g) fitted with a tap-funnel and sidearm adapter. The mixture was stirred at 25°C for 12 h; thereafter, the product was slowly washed with ethyl ether then water and dried over anhydrous Na_2SO_4 to give a white solid.

SI [3]: A mixture of methanolic solution of SI **[1]** (3.75 mmoles) was refluxed with L-histidine (5.16 mmoles) at 65°C for 24 h. The resulting product was washed with methanol (3 × 15 mL), filtered and dried overnight at 35°C to give a milky white solid.

SI [4]: Similarly, the methanolic solution of L-histidine (21.5 mmoles) and trans-androsterone (6.90 mmoles) were refluxed at 65°C for 24 h. The resulting products were washed with methanol (4 × 10 mL), filtered and dried overnight at 35°C to afford a white solid.

AUTHOR COPY

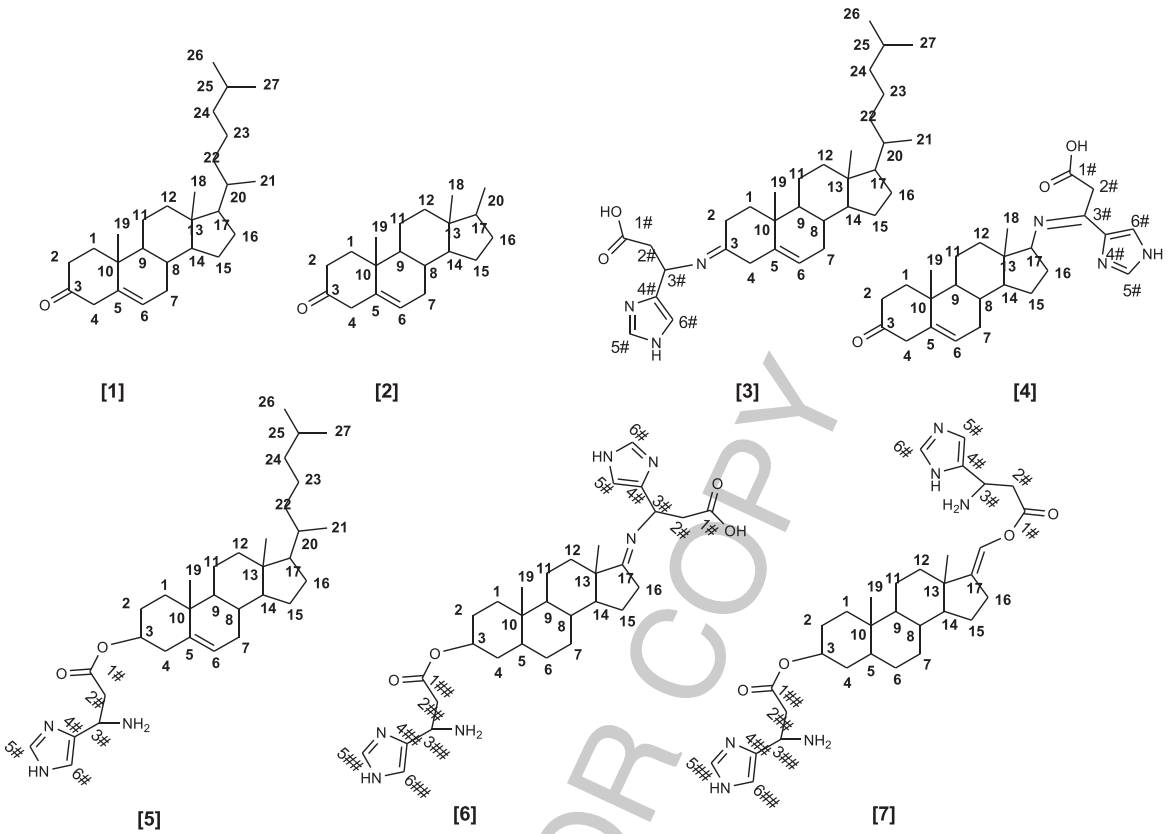


Fig. 1. Structural presentation of SIs [**1**–**7**].

SI [5–7]: A methanolic solution of L-histidine (6.75 mmoles) was mixed with cholesterol (5.17 mmoles), SI **[4]** (6.9 mmoles) and SI **[2]** (3.45 mmoles), respectively. The individual mixtures were refluxed in the presence of *p*-toluene sulphonic acid for 72 h in a closed system coupled to a 100 mL tap-funnel packed with anhydrous Na_2SO_4. The resulting products were evaporated to dryness, washed and dried overnight at 35°C. The structures of the seven SIs [**1**–**7**] are presented in Fig. 1.

3. Preparation of substrates and reagents

Substrate emulsion for conjugated diene assay was prepared by mixing 155 μL linoleic acid and 175 μg Tween-20 in 50 mL pH 7 phosphate buffer. Substrate solution for the α-amylase assay was prepared by adding 10 mg/mL of starch in 0.5 M Tris–HCl buffer (pH 6.9) and 0.01 M $CaCl_2$; preincubated at 37°C for 5 min. Substrate solution for the α-glucosidase assay was prepared by dissolving *p*-nitrophenyl glucopyranoside in 20 mM phosphate buffer solution pH 6.9. Stock solution of β-carotene/linoleic acid was prepared by adding 0.1 mg/mL of β-carotene in chloroform to a mixture of 40 mg and 400 mg of linoleic acid and Tween 40, respectively. The working concentrations (200–5000 μg/mL) of the various SIs were prepared and stored at 4°C. 2,2′-azino-bis (3-ethylbenzothiazoline-6-sulphonic acid (ABTS) was prepared from a mixture of 7 mM ABTS and 2.45 mM potassium persulfate. Iron-EDTA solution was prepared from 0.13% $(NH_4)_2Fe(SO_4)_2{\cdot}6H_2O$ and 0.26% EDTA. Iron-EDTA solution was prepared by mixing 0.13% ferrous ammonium sulphate and 0.26% EDTA.

AUTHOR COPY

4. *In vitro* oxidative species suppression assays

4.1. Lipid peroxidation inhibitory assay

According to Mitsuda, Yasumoto, & Iwami [17], a mixture of 100 μL solution of steroidal inhibitor (200 μg/mL), 2.4 mL phosphate buffer and substrate emulsion (2.5 mL) was pre-incubated for 30 min. Every 24 h, 100 μL aliquot of the above mixture was taken, mixed with 3.7 mL ethanol and 100 μL of mildly acidified 20 mM $FeCl_2$ solution. Afterward, the resulting mixture was treated with 100 μL of 30% $K_4[Fe(CN)_6]\cdot 3H_2O$ and the absorbance recorded at 500 nm. An emulsion of 2.5 mL linoleic acid and 2.5 mL phosphate buffer was used as blank.

4.2. Ferric ion reducing power (FRP)

In this assay, gallic acid was used as standard. The ferric reducing power of the SIs was investigated by adding 1.0 mL of working concentrations to 2.5 mL phosphate buffer pH 6 and 1% $K_4[Fe(CN)_6]\cdot 3H_2O$ [18]. Incubated at 50°C for 20 min, thereafter, 2.5 mL of 10% trichloroacetic acid (TCA) was introduced. Then, 2.5 mL aliquot of the mixture was taken and diluted twice with deionised water, before adding 0.5 mL of 0.1% $FeCl_2$. Absorbance was measured at 700 nm after 30 min of incubation. The ferric reducing power was measured and expressed as μg GAE/g.

4.3. Trolox equivalent antioxidant capacity (TEAC)

The ABTS radical cation solution was incubated in the dark at 25°C for 24 h before usage and diluted with methanol to a working absorbance of 1.8269 at 734 nm. The assay mixture was constituted with 3.5 mL of pre-equilibrated $ABTS^+$ at 30°C and 500 μL of Trolox solution (0.5–3.5 mg/mL) while the **SIs** (200 μg/mL) were similarly treated. The antioxidant capacities obtained from standard curves were expressed as μg/mL Trolox/g.

4.4. Conjugated diene assay

According to the protocol described by Kabouche, Kabouche, Öztürk, Kolak, & Topçu [19]; 3 mL aliquots of β-carotene/linoleic acid emulsion was mixed with 300 μL of the SIs working concentrations in a capped vial and incubated at 50°C for 60 min. The initial and final absorbances after 60 min were recorded at 700 nm followed by the estimation of the % β-carotene bleaching activity (% β-CBA).

4.5. Hydroxyl radical scavenging assay

In a tightly capped tube, a mixture of 1.0 mL of the SIs working concentrations, iron-EDTA solution, methanol (0.85% in 0.1 M phosphate buffer, pH 7.4), 0.5 mL of 0.018% EDTA, and 0.22% ascorbic acid was heated over a water bath at 85°C for 15 min. Further, about 1.0 mL of 17.5% ice-cold TCA was added to terminate the reaction; followed by 3.0 mL of Nash reagent. Afterward, the mixture was incubated for 15 min at 25°C [20]; absorbance measured at 412 nm against a reagent blank and expressed as % hydroxyl radical scavenging activity.

4.6. Nitric oxide radical scavenging assay

To generate the nitrite ion, a reaction mixture containing 3.0 mL of 10 mM sodium nitroprusside in phosphate-buffered saline (pH 7.4) and working concentrations of the SIs, were incubated at 25°C for 60 min [21]. Afterward,

AUTHOR COPY

5.0 mL of Griess reagent was introduced, and the absorbance of the chromophore (nitrite ion) left was measured at 546 nm against a reagent blank. The nitrite ions scavenging activity of the SIs were reported as % inhibition.

5. *In vitro* digestive enzyme suppression assays

5.1. α-Amylase suppression assay

Approximately 0.2 mL of the working concentrations of the SIs [**1–7]** were added into a series of vials containing 4.5 mL of the substrate solution. Afterward, 0.1 mL of porcine pancreatic amylase in Tris–HCl buffer (2 units/mL) was introduced to the tubes, incubated at 37°C for 10 min, and the reaction was terminated by the addition of 50% acetic acid (0.5 mL). The vials were centrifuged at 2000 rpm for 5 min at 4°C and absorbance of the supernatant measured at 595 nm [22]. The α-amylase inhibitory activity was estimated, and the efficacy expressed as the IC_{50} (μg/mL).

5.2. α-glucosidase suppression assay

The α-glucosidase suppression activity of the SIs was estimated using α-glucosidase from *Saccharomyces cerevisiae*. To a series of test tubes, a preincubating mixture of 100 μL of α-glucosidase (1.0 U/mL) and 50 μL of the SIs concentrations was added to 50 μL substrate solution to initiate the reaction. Afterward, the mixture was incubated further for 20 min and the reaction terminated by the addition of 2 mL of Na_2CO_3 (0.1M). The α-glucosidase activity was determined by measuring the absorbance of the mixture at 405 nm, and the efficacy of the SIs expressed as the IC_{50} (μg/mL) [23].

5.3. Statistical analysis

All data are presented as the mean ± SD. Statistical analyses were performed using one-way analysis of variance with OriginPro software Version 9.2.257. $P < 0.05$ was considered statistically significant.

6. Results and discussions

6.1. Synthesis of SIs

SIs [**5–7]** were prepared by the acetylation reaction between the free carboxylic acid of the L-histidine and the 3-hydroxyl group of cholesterol, SIs **[4** and **6]** resulting in yields of 33.7%, 98.1%, and 55.7%, respectively. Besides, the formation of SIs **[1** and **2]** was as a result of the strong oxidation and reduction of cholesterol and trans-androsterone with yields of 56.6% and 78.5%, respectively. However, SIs **[3** and **4]** were synthesised by the condensation of the α-amine group of the L-histidine and oxo groups of SI **[1]** at C-**3** and trans-androsterone at C-**27**; affording yields of 41.3% and 21.8%, respectively. Generally, the yields were well above average except for SIs **[4]** which may be due to steric factor and the kinetically favoured hydrolysis of SI **[5]**.

6.2. UV-visible and FTIR analysis of SIs [1–7]

The UV-visible absorption spectra of SIs **[2**, **3**, and **6]** were recorded in DMSO while [**1**, **4**, **5**, and **7**] were recorded in chloroform. The spectra of all the SIs exhibited intense bands ≤346 nm, which may be attributed to $\pi \longrightarrow \pi*$ and $n \longrightarrow \pi*$ transitions. The transitional bands were further confirmed by the characteristic stretching

AUTHOR COPY

vibrations of *O–H*, *C = O*, *C–O*, and *C = N* on the FTIR spectra of the SIs. Bands around 3350–3245 cm^{-1} are an indication of υ(O–H) at C-3 on the structure of **[2** and **4]**. More so, successful partial oxidation of the OH group at C-3 of cholesterol was indicated by the strong band around 1881 cm^{-1} associated with the $\upsilon(C=O)$ of cyclic ketone, leading to the formation of **[1]** [24, 25]. Also, the stretching vibrations around 1705–1695 and 1695–1684 cm^{-1} underline the existence of an azomethine and carbonyl bonds in the structures of **[3** and **4]** [26–28]. However, the spectra of SIs **[5–7]** revealed the presence of an acetate group at C-**1#** and **1##**, due to the stretching frequencies between 1735–1750 cm^{-1} and 1150–1350 cm^{-1} (Fig. S1).

6.3. NMR spectra of SIs [1–7]

SI **[1]:** yield: 33.7%; mp: 98–101°C and λ_{max}: 317 nm. FT-IR (cm^{-1}): 1637 (*C* = C) and 1881 (*C* = O); ^{1}H NMR (400 MHz, $CDCl_3$-*d*) δ 5.45 (tdt, *J* = 6.3, 1.9, 1.0 Hz, 1H), 3.11–2.98 (m, 2 H), 2.42–2.26 (m, 2 H), 2.05 (dt, *J* = 12.4, 7.0 Hz, 1 H), 1.97–1.85 (m, 2 H), 1.85–1.04 (m, 22 H), 1.15 (s, 3 H), 0.97–0.88 (m, 3 H), 0.82 (dd, *J* = 20.0, 6.7 Hz, 6 H), 0.66 (s, 2 H) (Fig. S2).^{13}C NMR (100 MHz, $CDCl_3$-*d*) δ 208.87, 166.04, 122.44, 56.69, 56.37, 50.71, 48.29, 42.56, 39.91, 39.30, 38.46, 36.73, 36.14, 35.75, 34.80, 31.93, 31.04, 28.18, 24.24, 24.11, 22.70, 20.88, 19.11, 17.57, 13.41 (Fig. S3). Elemental analysis calc. for $C_{27}H_{44}O$: C, 84.31%; H, 11.53%; %O, 4.16%. Found: C, 83.66%; H, 11.97%; O, 4.37%.

SI **[2]** yield: 78.5%, mp: 177–179°C, and λ_{max} 200 nm. FT-IR (cm^{-1}): 3412 (O–H) and 1235(C–O); ^{1}H NMR (400 MHz, DMSO–d_6) δ 4.26 (d, *J* = 6.9 Hz, 2 H), 3.67 (d, *J* = 13.2 Hz, 1 H), 3.61–3.53 (m, 1 H), 1.65 (s, 2 H), 1.54 (s, 1 H), 1.46 (s, 4 H), 1.32 (d, *J* = 5.4 Hz, 1 H), 0.81 (s, 4 H), 0.73 (s, 4 H) (Fig. S4). ^{13}C NMR (100 MHz, DMSO–d_6) δ 81.06, 68.99, 50.79, 44.71, 42.93, 41.91, 36.63, 36.35, 36.10, 35.69, 34.46, 30.67, 30.22, 29.90, 28.33, 23.36, 21.03, 13.11, 11.48 (Fig. S5). Elemental analysis calc. for $C_{19}H_{32}O_2$: C, 78.03%; H, 11.03%; O, 10.94%. Found: C, 77.48%; H, 11.67%; O, 10.85%.

SI **[3]**; yield: 41.3%, mp: 288–290°C and λ_{max} 335 nm. FT-IR (cm^{-1}): 3340 (*O* = H),1695 (*C* = N), 1635 (*C* = C), 1684(*C* = O) and 1312 (C–O); ^{1}H NMR (400 MHz, DMSO–d_6) δ 8.95 (dd, *J* = 7.6, 6.6 Hz, 1 H), 7.86 (dd, *J* = 7.6, 2.1 Hz, 1 H), 7.11 (dd, *J* = 6.6, 2.1 Hz, 1 H), 5.42 (tdt, *J* = 6.1, 1.9, 1.0 Hz, 1 H), 4.60 (t, *J* = 7.0 Hz, 1 H), 3.27 (qd, *J* = 12.4, 7.0 Hz, 2 H), 3.05 (dt, *J* = 1.6, 0.9 Hz, 2 H), 2.74–2.58 (m, 2 H), 1.94 (dddt, *J* = 12.4, 7.2, 6.2, 1.0 Hz, 1 H), 1.89–1.22 (m, 20 H), 1.22 (ddd, *J* = 5.9, 2.8, 1.5 Hz, 1 H), 1.22 – 1.17 (m, 1 H), 1.20–1.11 (m, 1 H), 1.15–1.02 (m, 1 H), 1.06 (s, 3 H), 0.96–0.88 (m, 3 H), 0.81 (dd, *J* = 20.0, 6.8 Hz, 6 H), 0.67 (s, 2 H) (Fig. S6).^{13}C NMR (100 MHz, DMSO–d_6) δ 191.32, 174.33, 141.57, 135.18, 134.63, 122.08, 121.49, 65.50, 56.74, 56.56, 50.57, 42.78, 39.91, 39.88, 39.26, 38.60, 36.21, 35.86, 34.95, 32.15, 32.06, 29.89, 29.82, 29.26, 28.19, 24.47, 24.08, 22.78, 21.10, 18.85, 18.82, 13.37 (Fig. S7). Elemental analysis calc. for $C_{33}H_{51}N_3O_2$: C, 75.96%; H, 9.85%; N, 8.05%; O 6.13%. Found: C, 75.38%; H, 10.44%; N, 8.66%; O, 5.52%.

SI **[4]**; yield: 21.8%, mp: 293–295°C and λ_{max} 340 nm. FT-IR (cm^{-1}): 3228 (O–H), 1695 (*C* = O), 1315 (C–O) and 1705 (*C* = N); ^{1}H NMR (400 MHz, $CDCl_3$-*d*) δ 9.94 (dd, *J* = 7.6, 6.6 Hz, 1 H), 7.87 (dd, *J* = 7.6, 2.2 Hz, 1 H), 7.09 (dd, *J* = 6.6, 2.1 Hz, 1 H), 4.59 (t, *J* = 7.0 Hz, 1 H), 3.71 (d, *J* = 7.9 Hz, 1 H), 3.71–3.59 (m, 1 H), 3.47 (dd, *J* = 12.4, 7.0 Hz, 1 H), 3.33 (dd, *J* = 12.4, 7.0 Hz, 1 H), 2.64–2.45 (m, 2 H), 1.87–1.34 (m, 21 H), 1.27 (qd, *J* = 7.0, 2.5 Hz, 1 H), 1.01 (s, 3 H), 0.81 (d, *J* = 1.3 Hz, 3 H) (Fig. S8). ^{13}C NMR (100 MHz, $CDCl_3$-*d*) δ 193.11, 174.51, 134.67, 134.57, 120.53, 69.60, 66.75, 53.68, 50.89, 44.20, 42.77, 37.63, 36.23, 35.75, 35.71, 35.05, 31.65, 30.94, 30.47, 30.01, 28.12, 24.28, 21.06, 18.10, 13.73 (Fig. S9). Elemental analysis calc. for $C_{25}H_{37}N_3O_3$: C, 70.22%; H, 8.72%; N, 9.83%; O, 11.23%. Found: C, 70.75%, H, 9.36%, N, 9.23%; O, 10.66%.

SI **[5]**: y obtained as a white solid; yield: 56.6%, mp: 244–246°C and λ_{max}: 310 nm. FT-IR (cm^{-1}): 1744 (*C* = O), 1695 (*C* = N), 1481–1122 (C–O) and 1634 (*C* = C); ^{1}H NMR (400 MHz, $CDCl_3$-*d*) δ 8.95 (dd, *J* = 7.6, 6.7 Hz, 1 H), 8.34 (dd, *J* = 7.6, 2.1 Hz, 1 H), 7.01 (dd, *J* = 6.6, 2.1 Hz, 1 H), 5.73 (d, *J* = 10.2 Hz, 2 H), 5.36 (tdt, *J* = 6.1, 1.9, 1.0 Hz, 1 H), 4.60 (p, *J* = 7.0 Hz, 1 H), 4.02 (tt, *J* = 10.2, 7.1 Hz, 1 H), 3.25–3.16 (m, 2 H), 2.41 (ddddd, *J* = 13.5, 12.4, 11.4, 7.0, 1.0 Hz, 2 H), 1.95–1.10 (m, 26 H), 1.04–0.88 (m, 7 H), 0.84 (d, *J* = 6.8 Hz, 3 H), 0.79 (d, *J* = 6.7 Hz, 3 H), 0.67 (s, 3 H) (Fig. S10). (100 MHz, $CDCl_3$-*d*) δ 134.88, 122.63, 119.91, 74.02, 56.74, 56.57,

AUTHOR COPY

54.95, 50.45, 39.91, 39.26, 38.28, 36.90, 36.21, 35.86, 32.12, 31.99, 30.39, 29.26, 28.19, 27.84, 24.47, 24.08, 22.78, 21.09, 19.28, 18.82, 13.37 (Fig. S11). Elemental analysis calc. for $C_{33}H_{53}N_3O_2$: C, 75.67%; H, 10.20%; N, 8.02%; O, 6.11%. Found: C,75.18%; H, 9.18%; N, 9.30%; O 6.34%.

SI **[6]**: obtained as a dirty white solid; yield: 98.01%, mp: 252–254°C, and λ_{max}: 346 nm. FT-IR (cm^{-1}): 3342 (O–H), 1715 (*C* = N), 1685 (*C* = O) and 1315 (C–O); ^{1}H NMR (400 MHz, DMSO-d_6) δ 8.93 (s, 2 H), 8.33 (s, 1 H), 7.87 (s, 1 H), 7.58 (s, 1 H), 7.11 (s, 1 H), 5.72 (s, 4 H), 4.76 (s, 1 H), 4.54 (s, 2 H), 4.02 (s, 1 H), 3.39 (s, 1 H), 3.32 (s, 1 H), 3.19 (s, 2 H), 1.33 (d, *J* = 10.8 Hz, 4 H), 1.00 (s, 6 H), 0.77 (s, 3 H) (Fig. S12). ^{13}C NMR (100 MHz, DMSO-d_6) δ 193.11, 174.68, 171.21, 135.45, 135.10, 135.02, 134.97, 121.58, 119.69, 73.66, 66.75, 55.29, 50.86, 50.55, 45.43, 42.37, 35.40, 35.28, 35.21, 34.97, 33.00, 32.04, 30.94, 30.39, 29.82, 28.04, 27.23, 23.79, 21.05, 16.99, 14.80 (Fig. S13). Elemental analysis calc. for $C_{31}H_{44}N_6O_4$: %C, 65.93; %H, 7.85; %N, 14.88; %O, 11.33. Found: %C 66.59, %H 7.38, %N 14.35; %O, 11.68.

SI **[7]**: obtained as a white solid; yield: 55.71%, mp: 275–277°C, and λ_{max} 274 nm. FT-IR (cm^{-1}): 1690 (*C* = O) and 1329 (C–O); ^{1}H NMR (400 MHz, $CDCl_3$-*d*) δ 8.95 (dd, *J* = 7.6, 6.6 Hz, 2 H), 8.34 (dd, *J* = 7.6, 2.0 Hz, 2 H), 7.59 (dd, *J* = 6.6, 2.1 Hz, 2 H), 5.71 (dd, *J* = 15.4, 10.2 Hz, 4 H), 4.77 (p, *J* = 7.0 Hz, 1 H), 4.60 (tq, *J* = 7.0, 1.5 Hz, 1 H), 4.01 (ttd, *J* = 10.2, 7.0, 3.1 Hz, 2 H), 3.28–3.14 (m, 4 H), 1.94–1.19 (m, 24 H), 0.89 (d, *J* = 1.4 Hz, 3 H), 0.77 (d, *J* = 1.4 Hz, 3 H) (Fig. S14). ^{13}C NMR (100 MHz, $CDCl_3$-*d*) δ 172.64, 171.21, 135.15, 135.10, 135.08, 135.02, 119.76, 119.69, 82.87, 73.66, 54.91, 54.87, 51.22, 45.01, 42.60, 35.60, 35.28, 35.18, 35.05, 33.00, 30.58, 30.55, 29.72, 27.71, 27.23, 27.04, 23.31, 20.74, 14.93, 12.12 (Fig. S15). Elemental analysis calc. for $C_{31}H_{46}N_6O_4$: C, 65.70%; H, 8.18%; N, 14.83%; O, 11.29%. Found: C, 65.09%; H, 7.66%; N, 15.65%; O, 11.77%.

The ^{13}C-NMR spectra of the seven SIs revealed the presence of a typical steroid backbone with C-1 to C-19 signals between 12.12–56.69 ppm [29] (Figs. S3–S15). Hydroxyl protons on SI **[4]** at C-**3** and SI **[2]** at C-**3** and C-**17** showed characteristic peaks at 3.73 ppm (dq, *J* = 8.6, 7.0 Hz, 1 H), and 3.45 ppm (dd, *J* = 12.4, 7.0 Hz, 1 H) [30], along with and the corresponding oxymethine carbons resonating at 69.59 ppm (Fig. S7), 68.98 ppm and 81.05 ppm (Fig. S5), respectively. Characteristic azomethine carbon signals were observed between 186.46–191.30 ppm for SIs **[3**, **4**, and **6]** [31, 32]. In addition, quaternary carbon of the oxo group at C-**1**# for SIs [**3**–**7**] (Figs. S7–S15) and C-**3** for **[1]** (Fig. S3) all signalled between 171.28–174.66 ppm. The NMR spectra evidence confirmed the presence of expected carbon and proton signals on the synthesized SIs.

6.4. Oxidative suppression activity

According to Singh et al., [33] lipid peroxidation of biological material results in the generation of hydroxyl radicals; leading to the formation of aldehyde derivatives. In this study, the lipid protective property of the seven SIs was evaluated according to Mitsuda et al., [34] (Fig. 2(a)).

It was observed that the protective activities of SIs **[1**, **5**, and **7]** were significantly weak; however, SIs **[2**–**4** and **6]** showed significant inhibition ($P < 0.05$) after day 5. There are slight similarities in the percentage inhibition of SIs [**2**–**4** and **6**] due to the closely related structural backbone. Further, a significant difference ($P < 0.05$) was observed in ferric reductive properties of SIs **[2**–**4** and **6]** with free proton coupled to the steroid backbone directly at C-**3** and/or C-**17** or indirectly through the α-carboxylic acid of the histidine residue in comparison to SIs **[1**, **5** and **7]**. However, [**5** and **7**] exhibited a relatively potent activity compared to [**1**] due to the intrinsic ability of the histidine residue to form stable chelates with the reductant Fig. 2(b)).

Also, the scavenging potential of the SIs for the ABTS radical cations; evaluated by monitoring the decolourisation of the blue-green chromophore revealed that the SIs were influenced by both the presence of histidine residue and free protons. Hence, there was a significant difference in the scavenging activities of SIs [**2**–**4**, and **6]** compared to SIs **[1**, **5**, and **7]** with neither a labile proton nor histidine residue (Fig. 3 (a)). A similar trend was observed on the potential of the SIs to prevent the oxidation of unsaturated fatty acid by ROS. The observed TEAC and β-carotene bleaching activity of SIs; suggests an entirely similar mechanism of suppression (Fig. 3 (b)).

AUTHOR COPY

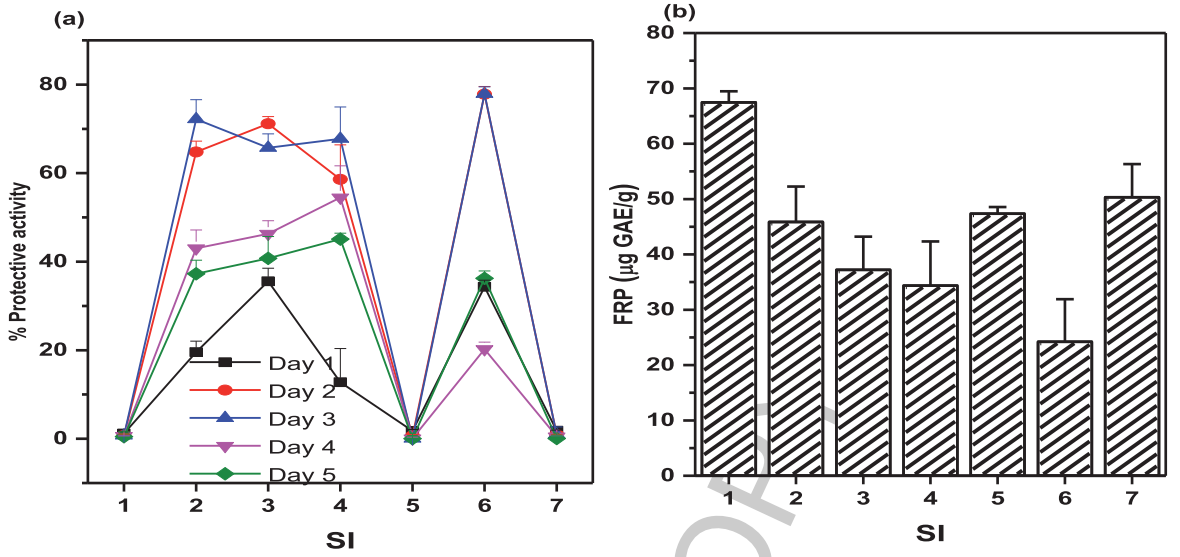


Fig. 2. (a) Lipid protective activity monitored at 500 nm for 5 days and (b) ferric reducing potential of SIs [**1**–**7**].

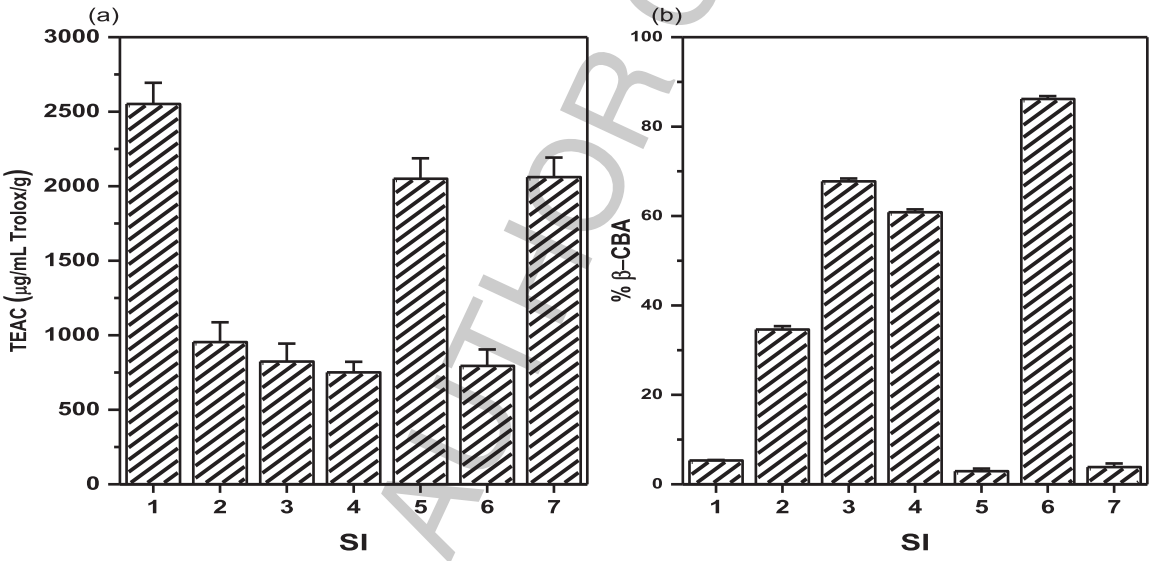


Fig. 3. (a) Trolox equivalent antioxidant capacity and (b) β-carotene bleaching activity of SIs [**1**–**7**].

Diffusible mediator like the hydroxyl and nitric oxide radicals which plays an effector molecule role in various physiological processes; causes cell damage/death. The scavenging activities of the SIs **[2**–**4**, **6**, and **7]** for the potent hydroxyl and nitric oxide pleiotropic mediators showed that significant amounts of aldehyde and stable nitrate compounds were still generated compared to SIs **[1** and **5]** (Fig. 4). This trend of inhibition exhibited by SIs **[6** and **7]** suggests that the mechanism of quenching these diffusible mediators is totally not dependent on the mechanism of lipid peroxide radical, ferric ion, $ABTS^{\pm}$ and bleaching of β-carotene suppressions. However,

AUTHOR COPY

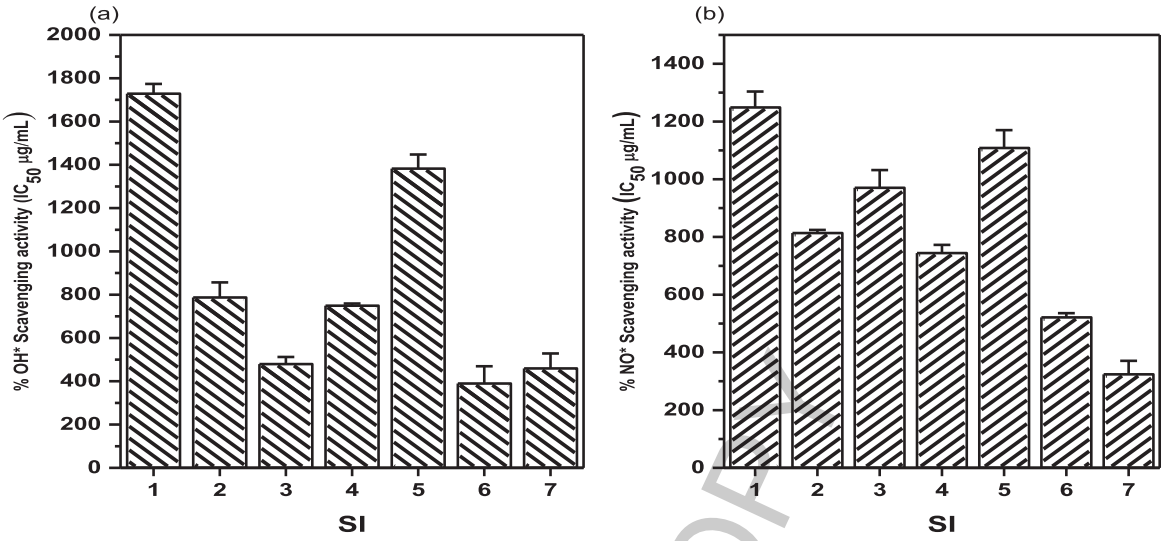


Fig. 4. (a) Hydroxyl radical scavenging activity and (b) Nitric oxide radical scavenging activity of SIs [**1**–**7**].

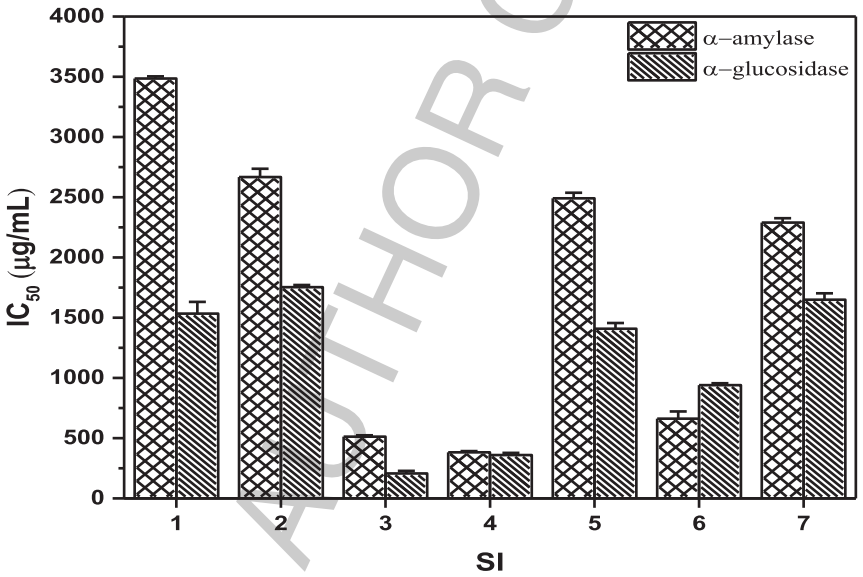


Fig. 5. Inhibitory potency of SIs [**1**–**7**] against α-amylase and α-glucosidase. Values are expressed as means ± SD of triplicate tests.

the presence of a facial π-system between C-**5** and C-**6** might offer a plausible scientific explanation to the observed mechanism. Consequently, the absence of the π-system and free protons on the steroid backbone are a major impediment to the activities of SI **[1]**. Generally, the activities of these SIs were Structure-Activity-Related (SAR); which are influential factors that drive the potency of SIs **[1–7]** towards the quenching of radicals and electron transfer.

AUTHOR COPY

7. Enzyme suppression activity

Our study showed that SIs **[3**, **4**, and **6]**, are effective inhibitors of α-amylase and α-glucosidase preventing the breakdown of starch into maltose and disaccharides into glucose, respectively (Fig. 5) [35]. Consequently, SIs [**3**, **4**, and **6]** showed a significant inhibition against the two digestive enzymes compared to the other SIs with IC_{50} values $\geq$1808.52 μg/mL (Fig. 5). Generally, SIs **[1**, **2**, **5**, and **7]** showed weak α-amylase suppression with moderate inhibition of α-glucosidase with no significant difference ($P > 0.05$) within the inhibitors.

Further, the suppression of α-glucosidase by SIs **[3**, **4**, and **6]** may be attributed to the possible enzymatic cleavage of the azomethine linkage (-C = N-) at C-**3** and C-**17** resulting in the increase in the concentration of histidine residue within the *in vitro* system; ultimately suppressing the production of glucose. According to a study by Kimura et al. [36], hepatic gluconeogenic enzymes and glucose production suppressions were linked to increased plasma histidine level.

8. Conclusion

The seven SIs were synthesised by simple template reaction and characterised with the aid of spectrophotometric methods. FT-IR information revealed the presence of azomethine, carbonyl, and hydroxyl characteristic peaks. In addition, these structural features were further confirmed by ^{1}H and ^{13}C NMR spectra. *In vitro* suppression evaluation of the SIs against α-amylase and the scavenging activities on radicals are influenced by the presence of labile protons at C-**3** and/or C-**17**. However, the ferric reducing potential and α-glucosidase suppression are influenced by the presence of enzyme-hydrolysable azomethine linkage. Generally, these SIs can find application as a nutraceutical in the management of oxidative diseases and diabetes mellitus via delayed activities of digestive enzymes; consequentially, lowering postprandial glucose absorption.

Acknowledgments

The authors extend their appreciation to the Directorate of Research and Institute of Chemical and Biotechnology, Vaal University of Technology, South Africa, for supporting the research.

Author contributions

Okoli B.J, Mthunzi F, and Modise S.J designed and supervised the entire experiments. The antioxidant and enzymes activity studies were executed by Olugbemi T.O and Okoli B.J, respectively. The spectroscopic analysis and interpretation of spectroscopic data were handled by Okoli B.J, James H, Ayo G.R, and Ndukwe, G.I. All authors participated in the writing, editing, and approval of the manuscript.

Conflict of interest

The authors have no conflicts of interest to declare.

AUTHOR COPY

Funding

This research received no external funding.

Supplementary Material

The supplementary material is available in the electronic version of this article: http://dx.doi.org/10.3233/MNM-190333.

References

[1] Land ET. Free radicals in biology and medicine. Fourth ed. International Journal of Radiation Biology. Oxford, UK: Clarendon; 1990;58:725-5.

[2] Sudha G, Priya MS, Shree RI, Vadivukkarasi S. In-vitro free radical scavenging activity of raw Pepino Fruit (*Solanum muricatum* Aiton). Int J Pharm Res. 2011;3(2):8-11.

[3] Geesin JC, Gordon JS, Berg RA. Retinoids affect collagen synthesis through inhibition of ascorbate-induced lipid peroxidation in cultured human dermal fibroblasts. Arch Biochem Biophys. 1990;278(2):350-5.

[4] Sajeeth CI, Manna PK, Manavalan R. Antioxidant activity of polyherbal formulation on streptozotocin-induced diabetes in experimental animals. Pelagia Res Libr. 2011;2(2):220-6.

[5] Khoddami A, Wilkes MA, Roberts TH. Techniques for analysis of plant phenolic compounds. Molecules. 2013;18(2):2328-75.

[6] Joyce DA. Oxygen radicals in disease. Adv Drug React Bull. 1987;127:476-9.

[7] Marx JL. Oxygen-free radicals linked to many diseases. Science (80). 1987;235(4788):529-31.

[8] Papas A. Antioxidant Status, Diet, Nutrition, and Health. 1st ed. Boca Laton, USA; CRC Press; 1998, 20-5.

[9] Wayner DM, Burton GW, Ingold KU, Locke S. Quantitative measurement of the total, peroxyl radical-trapping antioxidant capability of human blood plasma by controlled peroxidation. The important contribution made by plasma proteins. FEBS Lett. 1985;187(1):33-7.

[10] Shahidi F. Antioxidants in food and food antioxidants. Nahrung - Food. 2000;44(3):158-63.

[11] Arulpriya P, Lalitha P, Hemalatha S. *In-vitro* antioxidant testing of the extracts of Samanea saman (Jacq.) Merr. Pelagia Res Libr Der. 2010;1(2):73-9.

[12] Espinoza JL, Trung LQ, Inaoka PT, Yamada K, An DT, Mizuno S, et al. The repeated administration of resveratrol has measurable effects on circulating T-cell subsets in Humans. Oxid Med Cell Longev. 2017;2017.

[13] Rutkowski M, Grzegorczyk K. Adverse effects of antioxidative vitamins. Int J Occup Med Environ Health. 2012;25(2):105-21.

[14] Allen J, Bradley RD. Effects of oral glutathione supplementation on systemic oxidative stress biomarkers in human volunteers. J Altern Complement Med. 2011;17(9):827-33.

[15] Arcan I, Yemenicioğlu A. Antioxidant activity of protein extracts from heat-treated or thermally processed chickpeas and white beans. Food Chem. 2007;103(2):301-12.

[16] Cooperman JM, Lopez R. The role of histidine in the anemia of folate deficiency. Exp Biol Med (Maywood). 2002;227(11):998-1000.

[17] Mitsuda H, Yasumoto K, Iwami K. Antioxidative action of indole compounds during the autoxidation of linoleic acid. Eiyo To Shokuryo. 1966;19(3):210-4.

[18] Juntachote T, Berghofer E. Antioxidative properties and stability of ethanolic extracts of Holy basil and Galangal. Food Chem. 2005;92(2):193-202.

[19] Kabouche A, Kabouche Z, Öztürk M, Kolak U, Topçu G. Antioxidant abietane diterpenoids from *Salvia barrelieri*. Food Chem. 2007;102(4):1281-7.

[20] Klein SM, Cohen G, Cederbaum AI. Production of formaldehyde during the metabolism of dimethyl sulfoxide by hydroxyl radical generating systems. Biochemistry. 1981;20(21):6006-12.

[21] Mandal P, Misra TK, Ghosal M. Free-radical scavenging activity and phytochemical analysis in the leaf and stem of *Drymaria diandra* Blume. Int J Integr Biol. 2009;7(2):80-4.

[22] Hansawasdi C, Kawabata J, Kasai T. α-Amylase inhibitors from roselle (*Hibiscus sabdariffa* Linn.) Tea. Biosci Biotechnol Biochem. 2005;64(5):1041-3.

AUTHOR COPY

[23] Muhammad A, Jahangir M, Hussan S, Choudhary M. Inhibition of α-glucosidase by oleanolic acid and its synthetic derivatives. Phytochemistry. 2002;60(3):295-9.

[24] Mejin M. Isolation, structural elucidation and antibacterial activity of the chemical constituents of *Scaevola spinescens*. University of Adelaide,Adelaide, South Australia, 5005; 2009.

[25] Fuloria NK, Fuloria S. Analytical & bioanalytical structural elucidation of small organic molecules by 1D, 2D and multi dimensional-solution NMR spectroscopy. J Anal Bioanal Tech. 2013;S11(1):1-8.

[26] Sam N, Affan A, Salam A, Ahmad FB, Asaruddin MR. Synthesis, spectral characterization and biological activities of Organotin (IV) complexes with ortho -vanillin-2-hydrazinopyridine (VHP). Open J Inorg Chem. 2012;2012(April):22-7.

[27] Karrouchi K, Radi S, Ramli Y, Taoufik J, Mabkhot YN, Al-Aizari FA, et al. Synthesis and pharmacological activities of Pyrazole derivatives: A review. Molecules. 2018;23(1):134.

[28] Sahoo J, Kumar MS, Sudhir KP. Synthesis, spectral characterization of some new 3-heteroaryl azo 4-hydroxy coumarin derivatives and their antimicrobial evaluation. J Taibah Univ Sci. 2015;9(2):187-95.

[29] Bross-Walch N, Kühn T, Moskau D, Zerbe O. Strategies and tools for structure determination of natural products using modern methods of NMR spectroscopy. Chem Biodivers. 2005;2(2):147-77.

[30] Tebby JC. Two-dimensional NMR spectroscopy: Applications for chemists and biochemists (methods in stereochemical analysis, vol. 9). Eds. W. R. Croasmun RMKC, editor. Vol. 212, Analytica Chimica Acta. Weinheim, Wiley-VCH; 1988, 365.

[31] Reiss A, Chifiriuc MC, Amzoiu E, Spînu CI. Transition Metal(II) Complexes with Cefotaxime-Derived Schiff Base: Synthesis, Characterization, and Antimicrobial Studies. Bioinorg Chem Appl. 2014;2014:1-17.

[32] Akila E, Usharani M, Vimala S, Rajavel R. Synthesis, spectroscopic characterisation and biological evaluation studies of mixed ligand Schiff base with metal (II) complexes derived from o-phenylene diamine. Chem Sci Rev Lett. 2012;1:181-94.

[33] Singh HP, Kaur S, Negi K, Kumari S, Saini V, Batish DR, et al. Assessment of in vitro antioxidant activity of essential oil of *Eucalyptus citriodora* (lemon-scented Eucalypt; Myrtaceae) and its major constituents. LWT - Food Sci Technol. 2012;48(2):237-41.

[34] Hajdú Z, Hohmann J, Forgo P, Martinek T, Dervarics M, Zupkó I, et al. Diterpenoids and flavonoids from the fruits of *Vitex agnus*-castus and antioxidant activity of the fruit extracts and their constituents. Phyther Res. 2007;21(4):391-4.

[35] Kwon YI, Apostolidis E, Shetty K. Evaluation of pepper (*Capsicum annuum*) for management of diabetes and hypertension. J Food Biochem. 2007;31(3):370-85.

[36] Kimura K, Nakamura Y, Inaba Y, Matsumoto M, Kido Y, Asahara SI, et al. Histidine augments the suppression of hepatic glucose production by central insulin action. Diabetes. 2013;62(7):2266-77.

AUTHOR COPY